J Mater Sci (2012) 47:169–175
DOI 10.1007/s10853-011-5784-1

Spark plasma sintering synthesis and mechanical spectroscopy of the ω-$Al_{0.7}Cu_{0.2}Fe_{0.1}$ phase

G. Laplanche · P. Gadaud · J. Bonneville · A. Joulain · V. Gauthier-Brunet · S. Dubois · F. Jay

Received: 7 June 2011 / Accepted: 11 July 2011 / Published online: 28 July 2011

Abstract Starting from a mixture of Al–Cu–Fe quasicrystalline (QC) particles and Al powder, a fully dense and almost Al–Cu–Fe ω single-phase alloy was produced by spark plasma sintering. This technique allows synthesising large samples with sizes suitable for mechanical spectroscopy experiments. Mechanical spectroscopy was selected because it is a relevant tool for detecting the presence of structural defects at both nano and microscopic scales. Young's moduli were measured in the 15 kHz range as a function of temperature by the resonant frequency method. Young's moduli behave similarly for typical metals and exhibit values that are comparable to those of the Al–Cu–Fe QC phase. The damping coefficient Q^{-1} was determined at various temperatures between room temperature and 840 K over a large frequency range, i.e. between 10^{-3} and 10 Hz. The results suggest that solid friction effects do occur. In addition, a relaxation peak is observed in the intermediate temperature range.

G. Laplanche · J. Bonneville (✉) · A. Joulain · V. Gauthier-Brunet · S. Dubois · F. Jay
Département de Physique et Mécanique des Matériaux, Institut P' - Université de Poitiers - CNRS UPR 3346 - ENSMA, SP2MI - Téléport 2 - Boulevard Marie et Pierre Curie, BP 30179, 86962 Futuroscope Chasseneuil Cedex, France
e-mail: joel.bonneville@univ-poitiers.fr

P. Gadaud
Département de Physique et Mécanique des Matériaux, Institut P' - Université de Poitiers - CNRS UPR 3346 - ENSMA, 1 Avenue Clément Ader, BP 40109, 86961 Futuroscope Chasseneuil Cedex, France

Introduction

A recent study [1, 2] has shown that the flow stress of Al–base metal matrix composites (MMCs) initially reinforced by quasicrystalline (QC) Al–Cu–Fe particles was highly dependent on the synthesis temperature. It was earlier identified by Tsaï et al. [3] that the Al–Cu–Fe QC phase was stable for low-temperature (673 K) production process, while at high temperature (873 K), the QC phase transforms in the presence of the Al matrix into the crystalline ω-tetragonal phase. In both composites, plastic deformation has been identified as resulting from dislocation movements in the ductile Al matrix, and the difference in flow stress between the two composites has been ascribed to different spatial distributions of the reinforcement particles into the Al matrix [1]. The reinforcement particles are localised at grain boundaries in the composite reinforced by QC particles, referred to as Al/QC composite hereafter, and inside the Al grains in the composite reinforced by ω particles, referred to as Al/ω composite hereafter. Interfaces of different natures between the Al matrix and the reinforcement particles, i.e. crystal-QC interface and crystal–crystal interface in the two composites were in a first analysis ruled out from a purely mechanical point of view [1], but might also play a role in the stress enhancement of the Al/ω composite in comparison to the Al/QC composite [4].

A complete understanding of the mechanical properties of composite materials requires a precise knowledge of the mechanical properties of both the matrix and the reinforcement particles. The Al–Cu–Fe QC phase is rather well documented in the literature [for review, see 5]. It has been established [6] that it exhibits high hardness, high Young's modulus and high brittle-to-ductile transition temperature (BDTT) at approximately 0.7 T_m, T_m being melting

temperature [7]. Above the BDTT, the stress–strain curves show a yield point that is followed by a stage of strain softening only. The yield stress sharply decreases with increasing temperature over the range 700–1000 K by about two orders of magnitude, from nearly 1 GPa to 50 MPa [8]. On the contrary, the mechanical properties of the Al–Cu–Fe ω phase are poorly known, and only a few experimental results on the Al–Cu–Fe ω phase present in multi-phased materials have been published. The main reason is the difficulty of producing dense and monolithic samples of the ω phase.

In this study, we have used our expertise in producing Al-base MMCs reinforced by Al–Cu–Fe ω-phase particles to synthesise from a mixture of Al powder and Al–Cu–Fe QC particles the ω phase only. Preliminary results [9] indicate that the mechanical properties of the ω phase are similar to those of the QC phase, in particular the flow stress is strongly temperature-dependent, which suggests that thermally activated mechanisms are responsible for plastic flow. In this context, mechanical spectroscopy is a powerful tool for characterising elementary dislocation mechanisms and/or diffusion processes that might control plasticity. This article reports an ongoing study on the mechanical properties of the Al–Cu–Fe ω phase. It describes the production of bulk samples by spark plasma sintering (SPS) synthesis with suitable sizes for mechanical spectroscopy. The Young's moduli were measured at resonant frequency of approximately 15.5 kHz, from room temperature (RT) to 840 K. The related damping coefficient was also determined from this experiment. The damping coefficients measured over large ranges of both the frequency (10^{-3}–10 Hz) and the temperature (RT–840 K) are reported and discussed.

Experimental procedures

Synthesis and microstructural characterisation

A polyquasicrystalline ingot with nominal composition $Al_{0.635}Cu_{0.240}Fe_{0.125}$ was prepared by melting high-purity elements (>99.99%) under vacuum in an induction furnace, followed by drop casting into a water-cooled copper mould [10]. The ingot was subsequently annealed for 24 h at 1090 ± 10 K under high vacuum condition (10^{-3} Pa) and ball milled at 300 K during 40 min using a vibratory mill. The ball-to-powder mass ratio was set to be 10:1.

A commercially available Al powder (particle size <150 μm, 99% purity) and the QC-phase powder were separately sieved to obtain particles smaller than 80 μm. To ensure homogeneity, both powders were afterwards dry mixed in a Turbula for 1 h. The ω phase in this study is obtained from the chemical reaction of the original powders according to

$$4.20\ Al_{0.635}Cu_{0.240}Fe_{0.125} + 0.83\ Al \rightarrow 5\ Al_{0.695}Cu_{0.200}Fe_{0.105}, \quad (1)$$

by mixing 88 wt% of QC powder with 12 wt% of Al powder. Note that due to the original QC composition phase, the stoichiometric ω-$Al_{0.7}Cu_{0.2}Fe_{0.1}$ phase cannot be achieved. Then, the powder mixture was spark plasma sintered (SPSed) under vacuum condition (10^{-3} Pa) in a cylindrical graphite crucible (34 mm in diameter and 8 mm in height) at a set-up temperature of 873 K for 15 min under an axial pressure of 80 MPa for synthesising the ω-alloy. The set-up temperature is monitored by measuring the temperature on the external die wall with a pyrometer. Heating rate was monitored to achieve 100 K/min.

Density of the annealed QC-phase ingots, QC-phase powder and ω phase were measured by He pycnometry. Phase identification and lattice parameter measurements were performed by X-ray diffraction (XRD) using a Bruker D501 diffractometer with Cu-K_α radiations. Microstructure was examined by scanning electron microscopy (SEM) with a JEOL 5600LV microscope working at 20 keV. SEM observations were performed in the back-scattered electron mode to determine the phase distribution and their surface fraction. Local composition was measured by energy-dispersive X-ray (EDX) spectrometry using an Oxford Isis 300 EDX analyser. The results of EDX analyses are the average values over at least 20 individual analyses.

Mechanical testing

Beam samples of sizes 25 × 4 × 1.2 mm^3 were cut out from the SPSed compact and further mechanically polished with SiC papers of successive finer grades from 14 to 4 μm. It must be noted that the extreme brittle behaviour of the ω phase requires careful handling and dedicated sample holders. The Young's modulus E was determined using the resonant frequency technique in bending mode on the beam samples. In this technique, the samples are maintained by steel wires located at vibration nodes. Both excitation and detection are performed by an electrostatic device that measures the capacitance between the sample and the excitation electrode [11]. The tests were performed at a heating rate of 1 K/min under high vacuum (10^{-4} Pa) at strain amplitude lower than 10^{-6}. The resonance frequency F is determined by sweeping the excitation frequency with a network analyser in the appropriate frequency range. The Young's modulus E is calculated according to the relation:

$$E = 0.9464\ \rho\ F^2 \frac{L^4}{h^2} T\left(\frac{h}{L},\ \upsilon\right), \quad (2)$$

where F is in the 15 kHz range, ρ is the density, h and L are the thickness and gauge length of the sample, respectively, $T\left(\frac{h}{L},\ \upsilon\right)$ is a numerical factor slightly dependent on the

Poisson's ratio v, and for the present sample geometry, it is close to unity [12, 13]. The damping coefficient Q^{-1} is determined with the network analyser by measuring the bandwidth ΔF of the resonance peak at -3 dB from the relation [14]:

$$Q^{-1} = \frac{\Delta F}{F}. \quad (3)$$

The damping coefficient Q^{-1} was also measured using the low-frequency torsion technique. Measurements were performed under high vacuum with strain amplitudes of the order of 10^{-5}. The apparatus is an inverted pendulum allowing measurements at isothermal frequency sweep (forced vibrations in the range 10^{-3}–10 Hz). A special clamping system has been designed for studying brittle specimens [15].

The damping coefficient Q^{-1} in this study is given by the phase lag φ between the imposed sinusoidal stress and the resulting strain, which is determined by Fourier filter analysis with an accuracy of 10^{-4} according to the relation [14]

$$Q^{-1} = \tan(\varphi). \quad (4)$$

The main difference with the high-frequency technique is that anelasticity can be examined isothermally on stable microstructures over a wide range of frequencies. This technique is particularly well suited for accurately determining the activation energy associated with thermally activated mechanisms.

Results and discussion

Material

A representative XRD pattern of the SPSed compact is shown in Fig. 1. All the diffraction peaks are indexed according to the ω-$Al_{0.7}Cu_{0.2}Fe_{0.1}$ tetragonal structure. Lattice parameters and the resulting cell volume deduced from the peak positions are given in Table 1 for comparison with the other published data. Fig. 2 shows a SEM image of the SPS compact. In the backscattered electron mode, the difference in contrast is mainly sensitive to mass deviation. In Fig. 2, all the phases show very close contrast. The predominant grey areas correspond to the $Al_{0.693}Cu_{0.201}Fe_{0.106}$ composition, which is very close to the $Al_{0.7}Cu_{0.2}Fe_{0.1}$ composition of the ω stoichiometric phase. The composition of the darker grey area is $Al_{0.793}Fe_{0.181}Cu_{0.026}$, which corresponds to the λ-phase [10]. The bright grey areas correspond to i-$Al_{0.640}Cu_{0.234}Fe_{0.126}$ phase that did not transform. The QC and ω-phases have close compositions, which correspond to a mass deviation of nearly 6% only. Image analysis allows us to estimate that the QC-phase surface fraction is 4.3 ± 0.5%, while it is negligible for the λ phase.

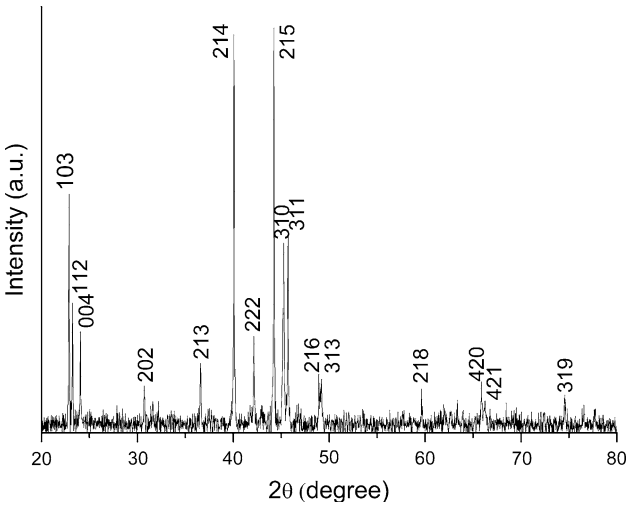

Fig. 1 XRD pattern of SPSed compact. All diffraction peaks are indexed according to the ω-$Al_{0.7}Cu_{0.2}Fe_{0.1}$ phase

The theoretical density of the ω phase, $\rho_{th,\omega}$ is given by the ratio of the mass of the unit cell, m_{uc} with respect to the corresponding volume, V_{uc}. Here, V_{uc} can be deduced from the lattice parameters a and c of the tetragonal ω phase determined by XRD, see Table 1. Bown and Brown [16] have established that the ω unit cell contains four $Al_7Cu_2Fe_1$ units. However, the EDX results show that the as-synthesised ω phase does not have the exact stoichiometric composition. It can be reasonably assumed that the ω-$Al_{0.693}Cu_{0.201}Fe_{0.106}$ composition corresponds to the substitution of 0.7 at.% Al by 0.1 at.% Cu and 0.6 at.% Fe, that is $\rho_{th,\omega}$ is then given by:

$$\rho_{th,\omega} = \frac{m_{uc}}{V_{uc}} = \frac{4\,(6.93\,M_{Al} + 2.01\,M_{Cu} + 1.06\,M_{Fe})}{N_A\,a^2 c} = 4.17\ \text{g/cm}^3, \quad (5)$$

where M_{Al}, M_{Cu} and M_{Fe} are the molar masses of Al, Cu and Fe elements, respectively, and N_A is Avogadro's number. The deduced theoretical value is slightly lower than the experimental density measured for the SPSed material, $\rho_{SPS} = 4.19$ g/cm^3 given in Table 2 compared with values found in the literature [17–19]. It is therefore necessary in Eq. 5 to take into account that the SPSed compact still contains QC-phase particles. Using the density of the QC phase given in Table 2 and a QC-phase volume fraction of 4.3% leads now to a theoretical density, ρ_{th}, of the SPSed compact of 4.19 g/cm^3 (Table 2), which accords better with the experimental value. Taking into account the inherent uncertainties on the measurements of both the He volume and the QC-phase volume fraction, it ensures a maximum porosity of 1%. Therefore, the SPS process allows for the production of fully dense material as confirmed by the measured density ($\rho_{SPS} = 4.19 \pm 0.01$ g/cm^3) which is equal to the theoretical density $\rho_{th} = 4.19 \pm 0.01$ g/cm^3,

Table 1 Lattice parameters and associated cell volumes of the ω-tetragonal phase (space group P4/mnc)

a (nm)	c (nm)	V (nm^3)	Reference
0.63393 ± 0.00009	1.4820 ± 0.0002	0.5956 ± 0.0003	Present work
0.633	1.481	0.5934	Phragmen [35]
0.6336 ± 0.0001	1.4870 ± 0.0002	0.5970 ± 0.0003	Bown & Brown [16]

within the standard deviations. ρ_{SPS} is also close to the density given by Tang et al. [20]. Figure 2 shows some bright grey areas that correspond to QC phase which did not react. There are possible explanations for the presence of the residual QC phase:

(1) The QC-phase excess might be due to local Al depletion in the green compact during the SPS process. While pyrometric measurements indicate a temperature of 873 K on the external die wall, it does not exclude temperatures higher than that of the melting point of Al. Both the measurement and the monitoring of temperature of the reactant powders are known as critical issues with the SPS technique [21]. Therefore, loss of molten Al may be expected by evaporation under vacuum condition leading to an excess of QC phase, which could not transform into ω phase according to reaction (1) [22].

(2) According to EDX results, the ω-phase composition is slightly heterogeneous from one area to another at the sample surface. The Al content of the ω phase may reach a concentration up to 71.6 at.% in many places, which is higher than the average Al content of 69.4 at.%. Therefore, the amount of Al may be locally insufficient to allow for the complete transformation of QC phase into ω phase.

Thus, it appears that using the SPS process necessitates a small excess of Al in the original powder mixture for obtaining a complete transformation of the QC phase into the ω phase. It must also be emphasised that the production of dense and monolithic ω phase would require that the presence of the λ-$Al_{0.765}Fe_{0.235}$ phase, which is observed as dark grey areas in Fig. 2 is avoided within the QC-phase alloy. The λ phase is already present in the QC-phase ingots, which are used for producing the QC-phase particles [10], and it has been found very stable during various heat treatments [1, 23].

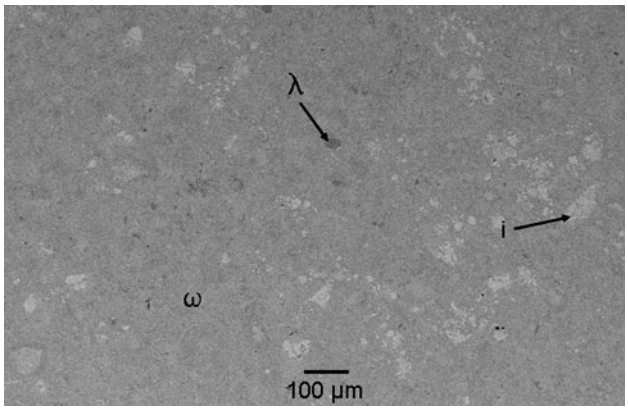

Fig. 2 SEM image of the SPSed compact, observed in the back scattered electron mode. At least three phases are identified, compositions of which according to EDX analysis correspond to ω, i and λ phases

Mechanical properties

High frequency measurements

Young's modulus and damping coefficient were measured from RT up to 840 K on the as-synthesized sample and after annealing at 840 K, i.e. after a first temperature run in Fig. 3. It must be emphasised that the experimental results are very reproducible over all the studied temperature

Table 2 Elastic modulus and density at 293 K of ω-phase, QC-phase and λ-phase (*LUPS* low uniaxial pressure sintering, *BS* Brillouin scattering, *RM* resonant method)

Phase	Processing	ρ (g/cm^3)	Composition	E measurement	E (GPa)	Reference
ω	SPS	4.19 ± 0.01	$Al_{0.693}Cu_{0.201}Fe_{0.106}$	RM	161 ± 1	Present work
	HIP	4.1 ± 0.1	$Al_{0.707}Cu_{0.194}Fe_{0.099}$	–	–	[3]
	HIP	4.18	–	Ultrasonic	168	[19]
	LUPS	5.540 ± 0.009	–	Nanoindentation	214 ± 10	[18]
i	Powder	4.73 ± 0.01	$Al_{0.611}Cu_{0.272}Fe_{0.117}$	–	–	Present work
	LUPS	–	$Al_{0.620}Cu_{0.255}Fe_{0.125}$	Nanoindentation	196 ± 5	[18]
	HIP	4.7	–	Ultrasonic	182	[19]
	–	–	$Al_{0.635}Cu_{0.245}Fe_{0.12}$	BS	172	[29]
	–	–	$Al_{0.65}Cu_{0.20}Fe_{0.15}$	RM	168	[28]
λ	–	–	$Al_{0.765}Fe_{0.235}$	–	130	[30]

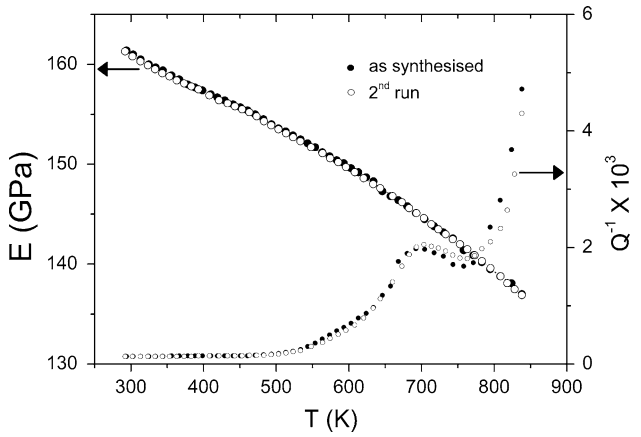

Fig. 3 Young's modulus E and damping coefficient Q^{-1} of the ω phase as a function of temperature

range, which clearly indicates that the microstructure of the SPSed ω phase is stable with respect to thermal cycling. Furthermore, we do not observe any transient effect on damping curves during the first heating or evolution of the Young's modulus values after annealing. Since this type of experiments is known to be very sensitive to the release of longitudinal internal stresses, it implies that residual stresses are not released during the first heating, as it is usually observed for other materials produced by hot isostatic pressing (HIP) or 'severe' forming techniques [24, 25].

The temperature dependence of Young's modulus behaves like that a typical metal, i. e. the slope is nearly constant at low temperature, and becomes steeper at high temperature. It can be reasonably assumed that, in the present case, the small density of porosities does not significantly influence the E value [26]. Its influence must be in the range of the experimental scatter, which is about ± 1 GPa. The E value of 161 ± 1 GPa measured at RT is comparable to that of the icosahedral (i) and λ phases [18, 19, 28–30] (see Table 2). E is in good agreement with the value measured by Tang et al. [27] using ultrasonic method, but differs from that given by Comte and Van Stebut [18]. For a polycrystalline sample, ultrasonic and the present resonant methods allow for the measurement of an elastic modulus E averaged over all crystallographic orientations. Comte and Van Stebut determined ρ, v and E using pycnometry, scanning acoustic microscopy and nanoindentation, respectively. Nanoindentation corresponds to local measurements, and the E value given by Comte and Van Stebut is then probably dependent on grain orientations. The value given by Comte and Van Stebut is close to the elastic modulus measured by Tang et al. [19] for the [214] crystallographic direction, $E_{214} = 204.5$ GPa, by neutron diffraction during in situ compression test. E_{214} is nearly 25% greater than E. Consequently, the difference between these values indicates that ω phase shows anisotropic elastic modulus, probably reflecting the high $c/a \sim 2.3$ ratio of the tetragonal structure.

Damping Q^{-1} curves show a relaxation peak located at approximately 710 K, which is superimposed onto a high temperature-dependent background. The damping level is low from 300 to 600 K in accordance with the brittle character of the ω phase [17]. According to Boltzmann's principle [14], the analysis of the dynamic parameters of the relaxation peak requires the decomposition of the spectra into two independent components, corresponding to the relaxation peak and the high background, respectively. Unfortunately, the peak height, of the order of 10^{-3}, is too small to allow an accurate decomposition. It also appears that the high background cannot be analysed in terms of a classic high-temperature background given by $F^{-1}e^{-H/kT}$ [14, 31], where H is the activation enthalpy of moving defects responsible of the damping and k is Boltzmann's constant. Consequently, a complementary study has been performed at low frequencies to further investigate this peculiar behaviour.

Low frequencies measurements

Isothermal damping measurements were performed as a function of frequency (from 10^{-2} to 10 Hz) from RT to 985 K (Fig. 4). To avoid possible metallurgical scatter, the sample was the same than the one used for high frequency measurements. At a given temperature, damping very slightly decreases with the frequency, in consideration of the logarithmic scale. Plotting the damping values as a function of temperature for two frequencies, 10^{-1} and 10 Hz, leads in Fig. 5 to the superposition of a peak onto an increasing background, similar to the one observed at high frequency. A striking feature is that there is practically

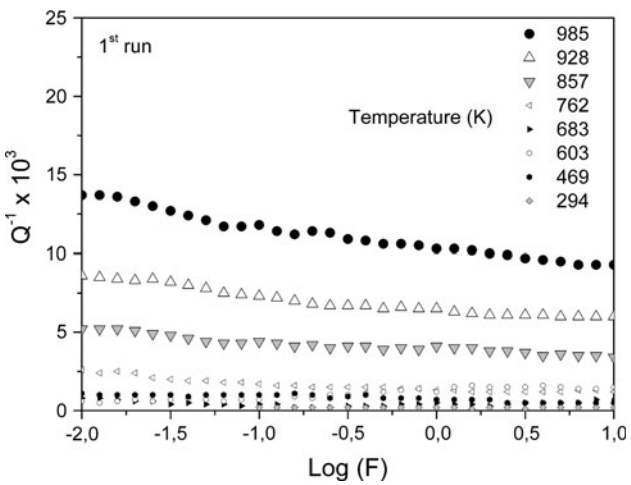

Fig. 4 Semi-logarithmic representation of the damping coefficient Q^{-1} obtained at different temperatures as a function of frequency

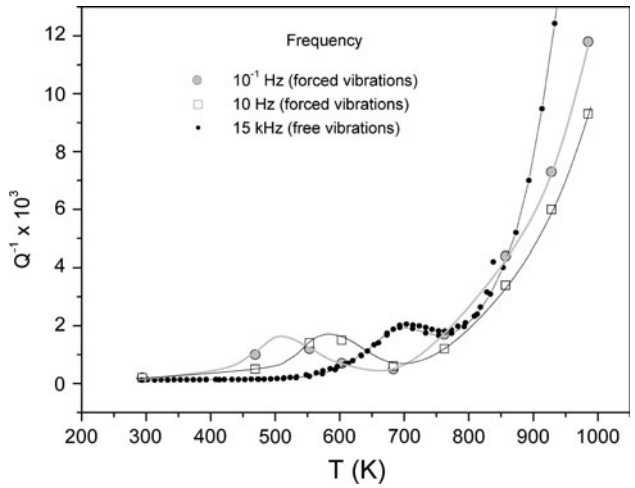

Fig. 5 Damping coefficient Q^{-1} of the ω phase as a function of temperature for three different frequencies

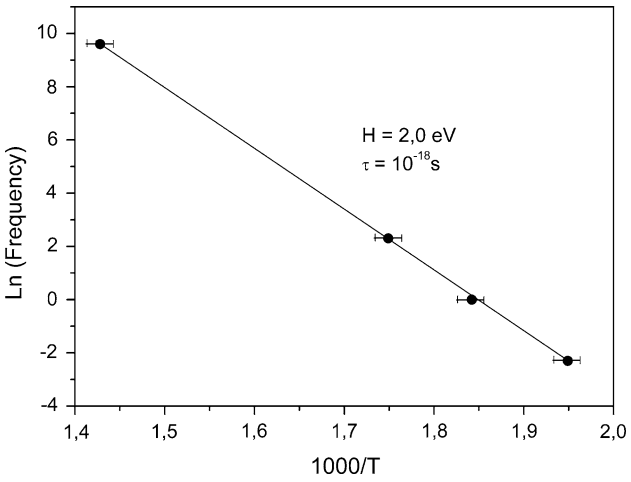

Fig. 6 Arrhenius type-plot of the relaxation peak frequency as a function of the reciprocal temperature

no temperature shift of the background, even when compared with high-frequency measurements. Consequently, the background cannot be associated, as suggested by high frequency measurements, with thermally activated mechanisms characterized by an exponential temperature dependence, but results from solid friction only. It is remarkable that a similar behaviour is recorded over five decades of excitation frequency and at temperature of nearly 700 K. The damping amplitude associated with this effect is, however, limited since the damping level does not exceed 10^{-2} at 985 K. Surprisingly, no other effect is detected, especially at high temperatures as might be expected in correlation with the brittle-to-ductile transition observed in microhardness tests [17]. Slight differences exist between damping spectra obtained at different frequencies (Fig. 5), but they probably arise from solid friction instabilities. For measurements performed at frequencies lower than 10^{-2} Hz, isothermal spectra become instable, and the sample must be heated and cooled for retrieving the same damping level, but some dispersion still remains. It can also be reasonably assumed that the cumulative time during the various tests performed at variable temperatures influences the damping level, which may lead to the differences observed in damping curves as well.

Solid friction effects have been reported in the literature on MMCs and on damaged materials [32, 33]. These effects have been only observed on very limited domains of frequency and temperature. Solid friction effects were ascribed to interface or free surface friction. At present, it is not yet possible to identify in this study the exact nature of interfaces that are, at microscopic scale, responsible of solid friction effects. Because no extended defects or structural damages have been observed by TEM [9], this leads us to assume that the specific nature of the particle–particle interfaces produced by the SPS sintering process are responsible of the solid friction effects.

Figure 5 allows us to determine the relaxation peak position in the medium temperature range, as a function of both the temperature and the frequency. Assuming that this peak corresponds to a single thermally activated process characterized by a relaxation time $\tau = \tau_0 e^{H/kT}$, where H is the activation enthalpy, and τ_0 is a characteristic time constant, then the peak position is given by the relation $2\pi\tau = 1$. Figure 6 represents the corresponding Arrhenius plot of the relaxation peak position as a function of the natural logarithm of the frequency from which the parameters H and τ can be extracted.

The characteristic time constant, or pre-exponential factor, $\tau_o \sim 10^{-18}$ s is much lower than the reciprocal of the Debye frequency, usually in the range 10^{-15}–10^{-14} Hz for metals, which indicates that the associated mechanism could be a Zener-type mechanism. It may correspond to stress-induced reorientation of substitutional defects, as observed for instance in the ordered alloys [34]. In this case, the activation energy $H = 2$ eV is the energy of diffusion of the substitution element.

Conclusion

The SPS technique has been used to produce almost fully dense and monolithic Al–Cu–Fe ω-phase material. Residual phases are the QC phase, that did not transform during the SPS process because of the lack of Al, and the λ phase, which is already present in the initial reinforcement particles. The latter phase was found very stable with respect to various Al-based MMC synthesis procedures [1, 23]. The advantage of the SPS technique in comparison with the hot isostatic pressuring method [17] is that it allows for the

production of large samples with suitable sizes for mechanical spectroscopy and for compression tests [9]. The Young's moduli of the ω phase prepared either by SPS or by HIP techniques are very similar and comparable to that of the QC phase [28]. Mechanical spectroscopy measurements suggest that damping results from solid friction effects. These effects rarely observed in mechanical spectroscopy are attributed to solid friction at particle interfaces. Finally, a relaxation peak due to point defect relaxation is found at intermediate temperature, which can be associated with a slight deviation from perfect chemical composition. A study is in progress to examine pre-strained samples with the aim of characterising by mechanical spectroscopy the damping associated with extended defects.

References

1. Laplanche G, Joulain A, Bonneville J, Gauthier-Brunet V, Dubois S, El Kabir T (2010) J Mat Res 25:957
2. Bonneville J, Laplanche G, Joulain A, Gauthier-Brunet V, Dubois S (2010) J Phys 240:012013
3. Tsaï AP, Aoki K, Akihisa I, Masumoto T (1993) J Mater Res 8:5
4. Taupin V, Berbenni S, Fressengeas C, Bouaziz O (2010) Acta Mat 58:5232
5. Bonneville J, Caillard D, Guyot P (2008). In: Hirth JP (ed) Dislocations in Solids, vol 14. Elsevier, North-Holland, pp 251–332
6. Bresson L, Gratias D (1993) J Non-Cryst Solids 153–154:468
7. Huttunen-Saarivirta E (2004) J Alloys Comp 363:154
8. Giacometti E, Baluc N, Bonneville J (1999) Phil Mag Lett 79:1
9. Laplanche G, Joulain A, Bonneville J, Gauthier-Brunet V, Dubois S to be published
10. Giacometti E, Fikar J, Baluc N, Bonneville J (2002) Phil Mag Lett 82:183
11. Mazot P, de Fouquet J, Woirgard J, Pautrot JP (1992) J Phys III:751
12. Spinner S, Reichard TW, Tefft WE (1960) J Res ASTM 64A:147
13. Spinner S, Tefft WE (1961) J Res ASTM 65A:167
14. Nowick AS, Berry BS (1972) Anelastic relaxation in solids. Academic Press, New York
15. Woirgard J, Mazot P, Rivière A (1981) J Phys 10:1135
16. Bown MG, Brown PJ (1956) Acta Crystallogr A 9:911
17. Laplanche G, Joulain A, Bonneville J, Gauthier-Brunet V, Dubois S (2010) Mat Sci Eng A 527:4515
18. Comte C, von Stebut J (2002) Surf Coat Technol 154:42
19. Tang F, Gnäupel-Herold T, Prask H, Anderson IE (2005) Mat Sci Eng A 399:99
20. Tang F, Meeks H, Spowart JE, Gnaeupel-Herold T, Prask H, Anderson IE (2004) Mat Sci Eng A 386:194
21. Molénat G, Durand L, Galy J, Couret A (2010) J Metall 2010:1
22. Yang C, Jin SZ, Liang BY, Jia SS (2009) J Eur Ceram Soc 29:181
23. Laplanche G, Joulain A, Bonneville J, Schaller R, El Kabir T (2010) J Alloys Comp 493:453
24. Gadaud P (2006) Int J Mater Prod Technol 26:326
25. Gadaud P, Pautrot S (2011) In: The 16th international conference on internal friction and mechanical spectroscopy (ICIFMS 16) held in Lausanne on July 3–8, 2011
26. Gadaud P, Pautrot S (2004) Mat Sci Eng A 370:422
27. Tang F, Anderson IE, Gnaupel-Herold T, Prask H (2004) Mat Sci Eng A 383:362
28. Tanaka K, Mitarai Y, Koiwa M (1996) Phil Mag A 73:1715
29. Vanderwal JJ, Zhao P, Walton D (1992) Phys Rev B 46:501
30. Köster U, Liu W, Liebertz H, Michel M (1993) J Non-Cryst Solids 153–154:446
31. Schoeck G, Bisogni E, Shyne J (1964) Acta Metall 12:1466
32. Rivière A, Gadaud P, Woirgard J (1993) In: Bhagat RB (ed) Damping of multiphase inorganic materials. ASM International, Materials Park
33. Pautrot S, Mazot P (1993) Revue de Métall 90:1665
34. Numakura H, Kurita N, Koiwa M, Gadaud P (1999) Phil Mag 79:943
35. Phragmen G (1950) J Inst Met 77:489